Applied Thermal Engineering 101 (2016) 284–292

Contents lists available at ScienceDirect

Applied Thermal Engineering

journal homepage: www.elsevier.com/locate/apthermeng

Research Paper

Thermal management for high power lithium-ion battery by minichannel aluminum tubes

Chuanjin Lan [a], Jian Xu [a], Yu Qiao [b], Yanbao Ma [a,*]

[a] School of Engineering, University of California, Merced, CA 95343, USA
[b] Department of Structural Engineering, University of California San Diego, La Jolla, CA 92093, USA

HIGHLIGHTS

- A new design of minichannel cooling is developed for battery thermal management system.
- Parametric studies of minichannel cooling for a cell are conducted at different discharge rates.
- Minichannel cooling can maintain almost uniform temperature ($T_{diff} < 1$ °C).
- Pumping power assumption is only about 5 milliwatt.

ARTICLE INFO

Article history:
Received 21 October 2015
Accepted 20 February 2016
Available online 4 March 2016

Keywords:
Electric vehicle
Lithium-ion battery
Thermal management
Minichannel cooling

ABSTRACT

Lithium-ion batteries are widely used for battery electric (all-electric) vehicles (BEV) and hybrid electric vehicles (HEV) due to their high energy and power density. An battery thermal management system (BTMS) is crucial for the performance, lifetime, and safety of lithium-ion batteries. In this paper, a novel design of BTMS based on aluminum minichannel tubes is developed and applied on a single prismatic Li-ion cell under different discharge rates. Parametric studies are conducted to investigate the performance of the BTMS using different flow rates and configurations. With minichannel cooling, the maximum cell temperature at a discharge rate of 1C is less than 27.8 °C, and the temperature difference across the cell is less than 0.80 °C using flow rate at 0.20 L/min, at the expense of 8.69e-6 W pumping power. At higher discharge rates, e.g., 1.5C and 2C, higher flow rates are required to maintain the same temperature rise and temperature difference. The flow rate needed is 0.8 L/min for 1.5C and 2.0 L/min for 2C, while the required pumping power is 4.23e-4 W and 5.27e-3 W, respectively. The uniform temperature distribution (<1 °C) inside the single cell and efficient pumping power demonstrate that the minichannel cooling system provides a promising solution for the BTMS.

1. Introduction

While the traditional transportation vehicle with an internal combustion engine contributes about 13% of annual world greenhouse gas (GHG) emissions [1], battery electric vehicles (BEV) and hybrid electric vehicles (HEV) are emerging replacements for traditional vehicles to reduce GHG emissions [2]. EVs and HEVs are not only cleaner and more environmentally friendly, but are also more economically effective as the operating cost is reduced dramatically [3]. Due to their high energy density, high power density, long life, and environmental friendliness, Li-ion batteries are widely used for BEVs and HEVs. However, poor performance at low temperature, degradation of electrodes at high temperature, and safety issues due to thermal runaway associated with the Li-ion batteries will directly influence the performance, cost, reliability, and safety of EVs. Therefore, a battery thermal management system (BTMS) is crucial for the EVs [4–10].

During thermal management study for lithium-ion batteries, adequate knowledge of heat generation and thermal behavior inside the battery is required to predict battery temperature. Studies have been done on the thermal modeling of batteries at different operating conditions, i.e., at normal discharge rates and thermal abuses [8,11–20]. For normal operating conditions, Pesaran et al. [11] developed a lumped capacitance battery thermal model to predict the thermal performance and impact of the temperature on vehicle level performance. Based on this lumped model, the thermal behavior of modules and packs were evaluated. In another study by Chen et al. [12], a detailed three-dimensional thermal model was developed to examine the thermal behavior of a lithium-ion battery, considering the layered-structure of the cell stacks, the case of a battery pack, and the gap between both elements. Using this detailed model, the asymmetric temperature profile and the anomaly of temperature

* Corresponding author. Tel.: +1 (209) 228 4046; fax: 209 228 4046.
E-mail address: yma5@ucmerced.edu (Y. Ma).

http://dx.doi.org/10.1016/j.applthermaleng.2016.02.070
1359-4311/

distribution on the surface can be simulated precisely. Besides these modeling techniques for normal conditions, different models were also developed for oven exposure testing. A one-dimensional predictive model for a 18,650 lithium-ion cell was developed by Hatchard et al. using the kinetics of jelly-roll material decomposition reactions [13]. To consider geometrical features, a three-dimensional model was developed by Kim et al. to determine the local hot spot propagation through the cell [14]. Their results showed that cell size greatly affected the thermal behavior of a cell due to different heat transfer area per unit volume. Guo et al. proposed another three-dimensional model to predict the thermal abuse performances of lithium-ion batteries with high capacity, and analyzed the temperature distribution under the abuse conditions [15]. The model predictions were compared to experimental test results and a good agreement was observed. For other abuse situations, thermal modeling for the battery pack has also been developed in a one-dimensional lumped model [16] and further in a three-dimensional model [17]. Thermal runaway caused by nail penetration was experimentally studied by Doh et al. [18] and Chiu et al. [19], who also modeled the complex reactions and mechanisms during the thermal runaway.

With profound understanding of the thermal behavior of battery cells at different operating conditions, different battery thermal management systems (BTMS), e.g., air cooling, liquid cooling, and phase change material (PCM) cooling, have been applied to avoid the safety issues from thermal aspect and to maintain the optimal operating temperature. Forced air cooling with different structures has been applied by manipulating the position of the air-inlet and the air-outlet along with longitudinal or horizontal battery packs [21–26]. However, compared with the effectiveness of passive cooling by PCM, the active forced air cooling is not a proper thermal management system to keep the temperature of the cell in the desirable operating range without expending significant fan power [27]. Another advantage of the PCM cooling is that the heat generated during the discharge can be stored as latent heat in the PCM and transferred back to the cell module during the relaxation. Therefore, the battery temperature can be kept above the environment temperature, which can increase the overall energy efficiency of the battery system [28–31]. Compared with the PCM cooling and air cooling, liquid cooling systems can provide more effective heat transfer with different channel designs [32–34]. The cold-plate structure of the S-type with guide plates was introduced by Zhang et al. to avoid the heat concentration and increase the heat transfer area [32]. To enhance the performance of the conventional channel with minimum pressure penalty, an oblique minichannel liquid cold plate was developed by Jin et al. to cool down the EV batteries without over-designing the cooling system [33]. In spite of these studies, a safer and more cost-effective thermal management system is still required.

In the present study, a new battery thermal management system using aluminum minichannel tubes was designed. Different designs of tube systems were parametrically studied at different discharging rates. The numerical modeling of the battery and cooling system design is introduced in the next section. To examine the performance of this BTMS at different discharge rates, different designs of tube systems are applied and the results are shown in the third section. The conclusion on the applicability of the minichannels cooling system is given in the last section.

2. Method

2.1. Physical problem

The computational domain consists of a prismatic geometry as the representative of one single battery cell, the minichannel cooling system, and the fluid. The dimensions for the cell are 173 mm (z: height) by 168 mm (x: width) by 39 mm (y: depth), and the capacity is

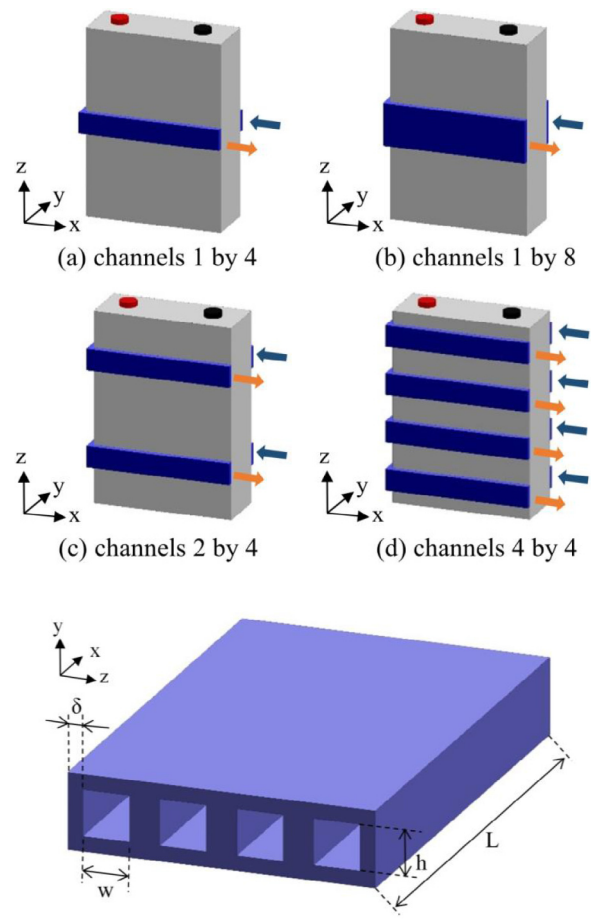

Fig. 1. Different designs of minichannel cooling system: (a) one strip with four minichannels; (b) one strip with eight minichannels; (c) two strips with four minichannels each; and (d) four strips with four minichannels each (blue arrows indicate the inflow direction and orange ones represent outflow direction); (e) details of the minichannel geometry.

55 Ampere-hours. The heat generation inside battery is assumed uniform, but the thermal conductivity is anisotropic. Other properties of the battery are assumed homogenous. The aluminum minichannel tubes wrap around three sides of the battery, as shown in Fig. 1(a)–(d). The geometry of the tubes is shown in Fig. 1(e): the height of channel (h) is 3 mm, and width (w) is 3 mm. The thickness of aluminum between the outer surface and channel (δ) is 1 mm, and the thickness between two neighbor channels will be twice δ [35]. With this minichannel cooling system, the temperature distribution across the battery is studied at different discharge rates. The desired temperature range for battery performance is between 15 °C and 35 °C [36]. If the battery temperature is below this range, battery performance will be lowered due to poor ion transport. On the other hand, a temperature higher than that range will cause faster side reactions, leading to higher dissipation rates of cyclable lithium and active materials.

2.2. Governing equations

The energy conservation equation of the battery cell is given as follows:

$$\rho_b C_b \frac{\partial T_b}{\partial t} = \frac{\partial}{\partial x}\left(k_x \frac{\partial T_b}{\partial x}\right) + \frac{\partial}{\partial y}\left(k_y \frac{\partial T_b}{\partial y}\right) + \frac{\partial}{\partial z}\left(k_z \frac{\partial T_b}{\partial z}\right) + Q_b \quad (1)$$

Table 1
Material properties [13,19].

Parameter	Aluminum	Battery
k (W m^{-1} K^{-1})	238	3.4 (cross-plane)/34.0 (in plane)
ρ (kg m^{-3})	2700	1700
C_p (J kg^{-1} K^{-1})	900	830

Table 2
Heat generation rate of 55 Ah lithium-ion battery monomer at different discharge rates [22].

Discharge rate	1C	1.5C	2C
Heat generation rate Q_b (W)	7.60	15.60	23.89

where ρ_b and C_b are the average density and average specific heat of the battery, respectively; k_x, k_z are the in-plane thermal conductivity along the width and height direction, and k_y is the cross-plane thermal conductivity in the depth direction. These battery material parameters are given in Table 1 [13,19]. Q_b is the uniform volumetric heat generation rate across the whole battery. Its value at different discharge rates for the lumped model of a single cell is extracted from Xu's work [22], as listed in Table 2.

Liquid water is used as the cooling fluid inside the aluminum minichannels. The energy conservation equation for water is:

$$\rho_w C_w \frac{\partial T_w}{\partial t} + \nabla \cdot (\rho_w C_w \vec{v} T_w) = \nabla \cdot (k_w \nabla T_w) \tag{2}$$

where ρ_w, C_w and k_w are the average density, specific heat and thermal conductivity of water, respectively. T_w is the water temperature and $\vec{v}$ is the velocity vector of water. The motion of incompressible liquid water is governed by the mass and momentum conservation equations:

$$\nabla \cdot \vec{v} = 0 \tag{3}$$

$$\rho_w \left[\frac{\partial \vec{v}}{\partial t} + (\vec{v} \cdot \nabla)\vec{v} \right] = -\nabla P + \mu \nabla^2 \vec{v} \tag{4}$$

where P and μ are the static pressure and dynamic viscosity of water.

2.3. Initial and boundary conditions

The initial temperatures of the battery, the cooling channels, and the water are set at 27 °C. At flow inlets, the velocity and temperature of water are assumed to be uniform and constant. For the flow outlet, a constant zero pressure is specified and an outflow boundary condition is used for energy equations. No slip boundary condition is used for the inside surfaces of minichannels. Thermal contact resistance between aluminum minichannels and the battery is not taken into consideration in this study. Since the battery is usually located in a narrow and tight space, the air surrounding the battery can be quickly heated up without effective ventilation. Therefore, in this study, convective cooling by surrounding air is assumed to be negligible in the situation of having no fans installed. In other words, a thermal insulation boundary condition is applied to all the outer surfaces of the battery. As a result, the minichannel cooling is the only way for the heat dissipation of the battery.

2.4. Numerical method

The commercial finite element software package COMSOL is used to solve the conjugate heat transfer problem. Each simulation is performed in two steps. In the first step, flow fields are solved using a stationary iterative solver with relative tolerance set as 0.001, since the effect of heat transfer on flow fields is quite small and can be neglected (water density is assumed constant). After the convergence of flow fields, in the second step, the heat transfer in both solid domain and fluid domain are solved together. Direct solver is used for time dependent simulation and the absolute tolerance is set as 0.001. Time step is set as one second since temperature field advances smoothly and monotonously. In this way, the simulation can be much faster than solving coupled flow and heat equations.

2.5. Model validation

In this study, free tetrahedral mesh is used for the mesh construction. A mesh independence check is first performed. Most elements are assigned to the fluid domain and the meshes at two corners are specially refined. Sparse mesh is used for the heat transfer in the solid battery domain. Two meshes with different numbers of elements are used for the mesh independence check. The geometry in Fig. 1(a) is used for the validation case. Uniform inlet velocity is set as 0.023 m/s and the discharge rate is 1C (Q_b = 7.60 W). For the fine mesh, 418,192 elements are used in total, 303,492 of which are used for fluid domain. For the coarse one, 202,778 elements are used in total, 135,312 of which are used for fluid domain. For the results, the maximum velocity obtained by fine mesh is 0.0378 m/s and pressure drop is 34.54 Pa. The maximum temperature in the battery is 34.87 °C. Using the coarse mesh, the maximum velocity obtained is 0.0374 m/s and pressure drop is 35.63 Pa. The maximum temperature in the battery is 34.57 °C. The difference in the maximum velocity and difference in maximum temperature are both 1%, while the pressure difference is about 3%. These results validate the mesh independence, and the coarse mesh design is used in this study.

After validating the mesh design, the numerical result of heat transfer and laminar flow also needs validation. As for the heat transfer simulation, energy conservation can be checked for the whole system. The input heat generation rate is 7.60 W from the battery at a discharge rate of 1C, and the thermal power carried away by the water is 7.67 W, which is the only option for heat loss from the system. The difference is 1%, thus validating the results for energy conservation. As for the laminar flows inside minichannels, the friction loss at the end of the long section before reaching the bend can be compared with analytical solutions. The long straight section of the minichannel is long enough for the flow to be fully developed before reaching the bend. For fully developed laminar flow inside rectangular channels with geometrical aspect ratio α (w/h), the friction factor (f) can be predicted by [37]:

$$(f\,\mathrm{Re})_{fd} = 24(1 - 1.3553/\alpha + 1.9467/\alpha^2 - 1.7012/\alpha^3 + 0.9564/\alpha^4 - 0.2537/\alpha^5) \tag{5}$$

where Re is Reynolds number and f is Darcy friction factor, respectively, given as: $\mathrm{Re} = \rho_w U_0 D_h/\mu$, and $f = (\Delta P * D_h)/(\frac{1}{2}\rho_w U_0^2 * 4L)$. D_h is the hydraulic diameter of the rectangular minichannel, U_0 is the average velocity at the channel inlet, μ is the dynamic viscosity of water, ΔP is the pressure drop, and L is the length. For a square duct, $(f\,\mathrm{Re})_{fd}$ is calculated to be 14.23 as $\alpha = 1$. The result from simulations is $f\,\mathrm{Re} = 13.36$, which differs from predictions by 6%.

In the end, the pressure drop of laminar flow through the whole minichannel with two 90° bends is calculated and the result is compared with theoretical predictions. To account for the entrance length effect, the apparent friction factor is calculated for both the developing and fully developed laminar flow regions in the channel, given as

$$f_{app}\,\mathrm{Re} = \left[\left\{ 3.2/(x^+)^{0.57} \right\}^2 + (f\,\mathrm{Re})^2_{fd} \right]^{\frac{1}{2}} \tag{6}$$

In this equation, entrance length is defined as: $x^+ = L/(D_h \cdot \mathrm{Re})$. More details for theoretical predictions are given in Liu's work [38].

As for the excess pressure loss due to 90° square bends, for slow flow or negligibly small Re, the pressure loss is linear in the velocity rather than quadratic, given as [39]:

$$\Delta P_{excess} = K_L \frac{\mu U_0}{D_h} \tag{7}$$

where K_L is the coefficient given for different bend geometries, which is 4.2 for a 3D square corner [39]. To validate the pressure loss based on this equation, a small inlet velocity is applied as $U_0 = 0.00579$ m/s. The total pressure loss calculated from simulation is 6.58 Pa, which is 6% different from the predicted value 7.03 Pa based on Eq. (5), (6) and (7). All the above mentioned tests for energy conservation and pressure drop comparison indicate that the numerical model used in this study is valid.

3. Results and discussions

After validating the numerical model, the effects of different minichannel designs at different discharge rates, as well as the effects of different flow rates, are studied here. The maximum temperature of the battery and the temperature difference between the maximum temperature and minimum temperature of the battery, denoted as T_{max} and T_{diff}, will be mainly discussed for different cases. Uniformity index T_{uni}, which is used to quantify the temperature difference inside the whole battery is also discussed. It is defined as:

$$T_{uni} = T_{diff} / T_{avg} \tag{8}$$

where T_{avg} is the average temperature of the whole battery. According to the definitions, the smaller these values are, the better performance it is for the thermal management system design.

3.1. Thermal management at a discharge rate of 1C ($Q_b = 7.60$ W)

3.1.1. Different designs for minichannel system

Four different minichannel cooling systems with a different number of strips and a different number of minichannels are chosen to study the effect of different geometric designs, as shown in

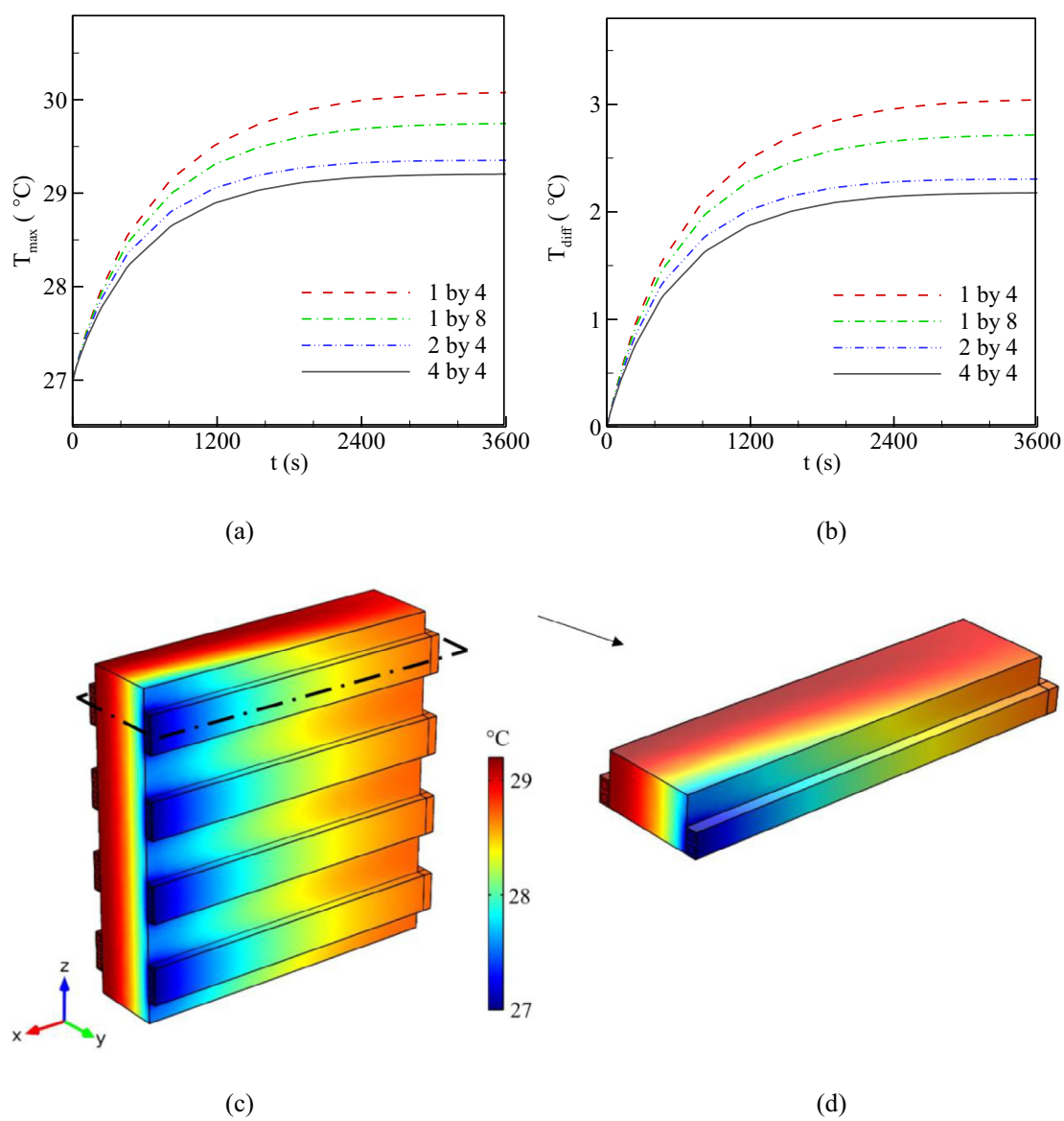

Fig. 2. (a) Temporal history of maximum temperature; (b) temporal history of temperature difference; (c) temperature distribution after 1 hour of discharging at 1C ($Q_b = 7.60$ W) with a flow rate at 0.05 L/min; (d) temperature distribution of the top one-eighth of the battery. Since no heat flux goes through the dashed plane in (c) due to symmetry and the thermal insulated outer surfaces of the battery, the simulation can be performed on this much smaller geometry than the original whole shape, thus saving computational resources and showing enlarged views.

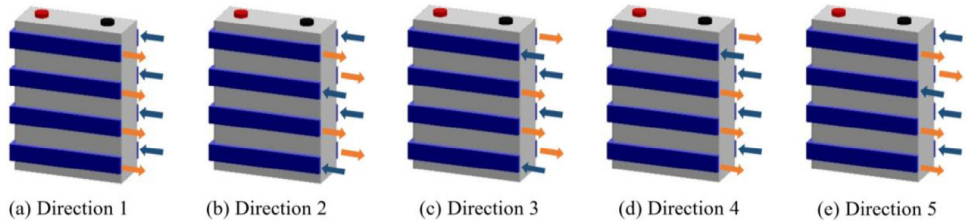

Fig. 3. Design with different flow directions. Blue arrows indicate the flow inlet and orange ones represent flow outlet.

Fig. 1(a)–(d). In design (a), one strip with four minichannels is wrapped in the middle of the battery; in design (b), one strip with eight minichannels is used; in design (c), two strips with four minichannels each are located in the upper and lower parts of the battery, respectively; in design (d), four strips with four minichannels each are distributed uniformly. All the flow inlets are set on one side of the battery and flow outlets on the other side.

The maximum temperatures of the battery T_{max} for the four different designs are shown in Fig. 2(a). The discharge rate is fixed at 1C (Q_b = 7.60 W), and the flow rate is 0.05 L/min. Since the total number of minichannels is different for designs (a)–(d), the inlet flow velocity varies accordingly for different designs due to different total cross-section areas. Design (a), which uses one strip with four minichannels, shows the highest temperature rise from 27.0 °C to 30.08 °C, after 1 hour of discharging. Compared to design (a), T_{max} for design (b) (one strip with eight minichannels) changes from 27.0 °C to 29.75 °C. This indicates that a strip with more minichannels can reduce the temperature rise, though the flow rate is lower. For design (c), which has the same total number of minichannels as design (b), T_{max} increases from 27.0 °C to 29.35 °C. This temperature increase is smaller than that of design (b). From the comparison between design (b) and design (c), it can be seen that a wider distribution of minichannels has better thermal management performance than concentrating all minichannels at one place. For design (d), which has four strips evenly distributed, T_{max} has the minimum increase from 27.0 °C to 29.20 °C. These results show that the design using more minichannels and a wider distribution has the minimum temperature increase. This is reasonable since the heat can be more easily dissipated by minichannels when the contact areas are larger and more distributed.

The temperature differences T_{diff} across the whole battery are shown in Fig. 2(b). It can be seen that the temporal change of T_{diff} is similar to T_{max} for each corresponding case. This is because near the minichannels inlet, the local battery temperature is always close to the inlet water temperature since the battery and the inlet water are only separated by a thin layer of aluminum (Fig. 2(c)). However, near the minichannels outlet, as the water is warmed up, the heat dissipation efficiency for the battery is reduced and the maximum battery temperature occurs. Since the local battery temperature near the minichannels inlet is the minimum battery temperature and remains almost unchanged after 1 hour of discharging, the variation of temperature difference depends mainly on the maximum temperature variation. T_{diff}, T_{max} and T_{uni} after 1 hour of discharging at 1C are shown in Table 3, as well as pressure drop and pumping power required. The pumping power for design (a) is more than 5 times larger than design (b), and more than 23 times larger than design (d). From the comparison in Table 3, design (d) requires minimum pumping power and obtains the best thermal management performance (minimum T_{diff}, T_{max} and T_{uni}), while the only shortcoming is the cost of the channel materials. Therefore, design (d) will be used for all the remaining subsections.

3.1.2. *Different flow directions for performance enhancement*

Based on design (d) in Fig. 1(d), five designs with different flow directions are compared to study the effect of flow direction, as shown in Fig. 3. The blue arrows indicate the flow inlets, and the orange arrows indicate the flow outlets. The design "Direction 1" has been used in Subsection 3.1.1.

The temporal variations of T_{max} and T_{diff} are shown in Fig. 4. Similar trends for T_{max} and T_{diff} are observed for all cases. Among the five

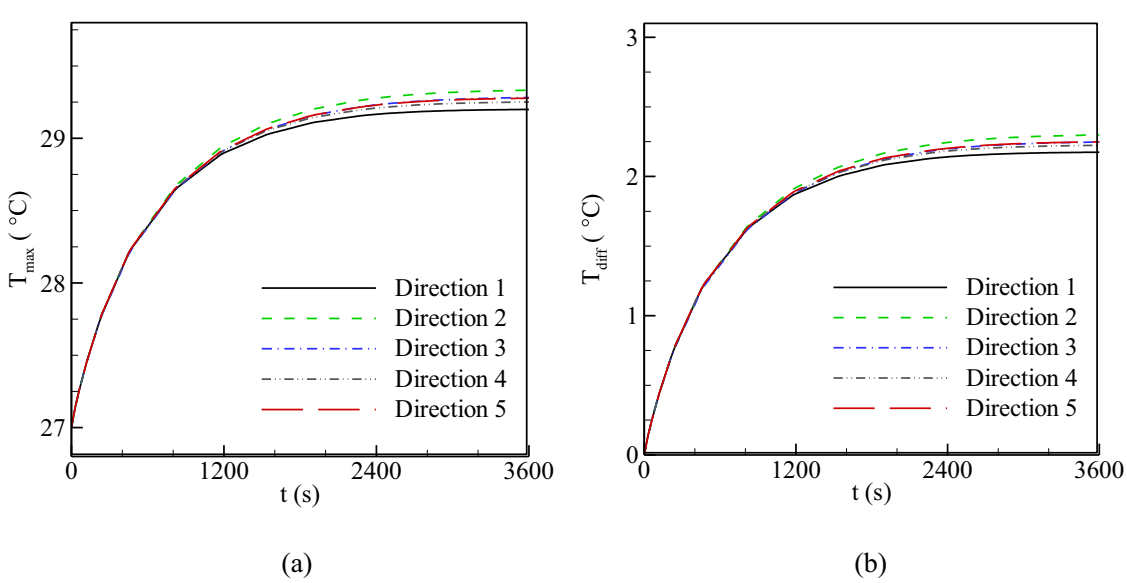

Fig. 4. Temporal history of (a) maximum temperature and (b) temperature difference using different flow directions, at a discharge rate of 1C (Q_b = 7.60 W).

Table 3
Comparison of pressure drop, pumping power, temperature difference, maximum temperature and uniformity index for different designs at a discharge rate of 1C (Q_b = 7.60 W) with a flow rate at 0.05 L/min.

Case	ΔP (Pa)	*Pumping Power* (W)	T_{diff} (°C)	T_{max} (°C)	T_{uni}
1 by 4	41.8	8.71e-6	3.04	30.08	0.102
1 by 8	15.8	1.66e-6	2.72	29.75	0.093
2 by 4	15.8	1.66e-6	2.30	29.35	0.079
4 by 4	7.03	3.66e-7	2.18	29.20	0.076

designs, case 'Direction 1' obtains the minimum T_{max} and T_{diff}. Considering the complexity and cost of the inlet manifold, the case 'Direction 1' is also the best choice. The worst thermal performance occurs for case 'Direction 2', which has alternative flow direction. For the other three cases, variations of T_{max} and T_{diff} show close performance. Based on these results, the design 'Direction 1' will be used for all the remaining subsections.

3.1.3. Different flow rates for performance enhancement

Since the pressure drop and the required pumping power are quite small as observed in Table 3, the flow rate can be increased to further improve the thermal management performance. In this study, the flow is kept in laminar regime.

The maximum temperatures and temperature differences of the battery at different flow rates are shown in Fig. 5. It can be seen that T_{max} and T_{diff} get lower as the flow rate increases. Using flow rates as 0.15 L/min and 0.20 L/min, T_{max} becomes stable in no more than 1200 s. From Fig. 5(c), it can be seen that the high temperature area of the battery is close to the minichannel outlet, since the water near the outlet is already heated up and the water temperature is close to the maximum temperature of the battery. When flow rate is 0.15 L/min, T_{max} is kept at 28 °C and T_{diff} is less than 1 °C. Once the flow rate is increased to 0.20 L/min, T_{max} gets to 27.81 °C and T_{diff} becomes 0.80 °C after 1 hour of discharging at 1C (Q_b = 7.60 W). As the flow rate increases, the uniformity index T_{uni} also reduces as T_{max} and T_{diff}, as shown in Table 4. These results demonstrate that the minichannel cooling system can maintain T_{diff} to be less than 1 °C, and it only requires 4.28e-6 W and 8.69e-6 W pumping power for 0.15 L/min and 0.20 L/min flow rate, respectively.

3.2. Thermal management at a discharge rate of 1.5C (Q_b = 15.60 W)

In this subsection, the thermal performance for a higher discharge rate at 1.5C (Q_b = 15.60 W) is studied. Based on the results in Subsection 3.1, flow rates higher than 0.20 L/min are used. The results are shown in Fig. 6. Both T_{max} and T_{diff} decrease as the flow rate increases; however, the effect of flow rate on cooling performance gets smaller as flow rate increases. From Fig. 6(c), it can be seen that the high temperature area of the battery is near the center of the battery in cross-plane (y) direction, slightly closer to the minichannel outlet. Due to the high flow rates used, the outlet temperature of the minichannel is much lower than the maximum temperature of the battery. When the flow rate increases from 0.20 L/min to 0.40 L/min, the T_{max} drops from 28.66 °C to 28.16 °C

Table 4
Comparison of pressure drop, pumping power, temperature difference, maximum temperature and uniformity index using different flow rates at a discharge rate of 1C.

Flow rate (L/min)	ΔP (Pa)	Pumping power (W)	T_{diff} (°C)	T_{max} (°C)	T_{uni}
0.05	7.03	3.66e-7	2.18	29.20	0.076
0.10	15.8	1.64e-6	1.31	28.32	0.047
0.15	27.4	4.28e-6	0.97	27.98	0.035
0.20	41.8	8.69e-6	0.80	27.81	0.029

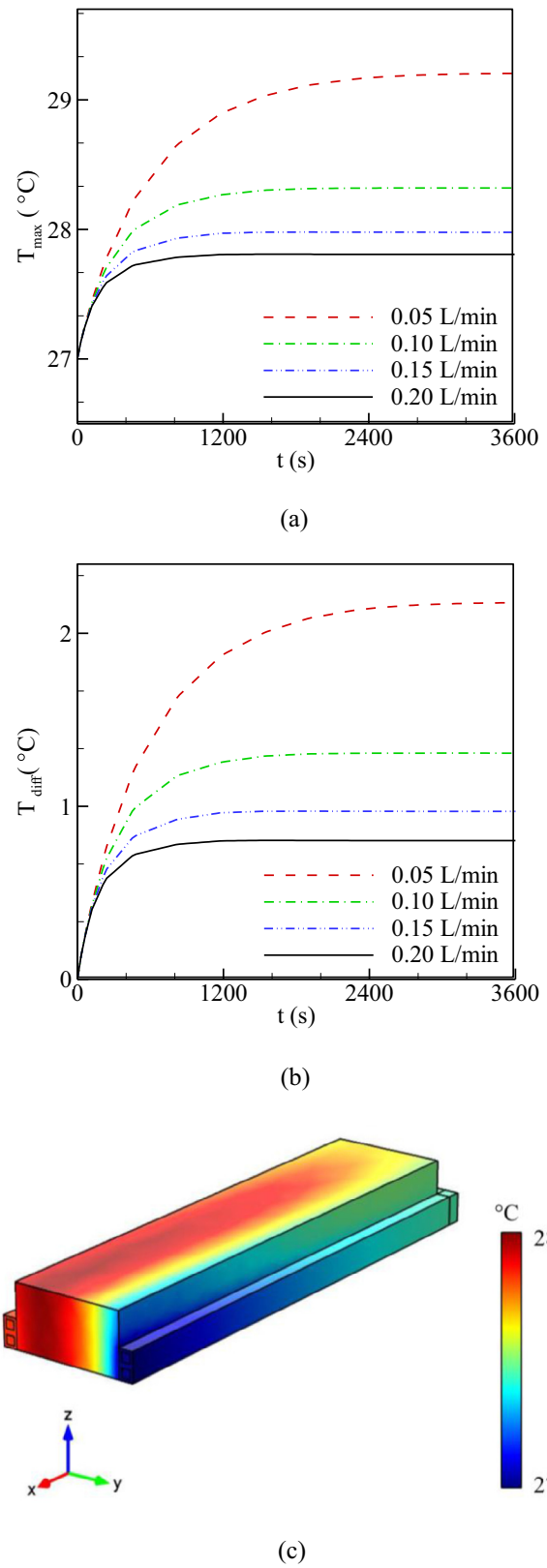

Fig. 5. Temporal history of (a) maximum temperature and (b) temperature difference using different flow rates, at a discharge rate of 1C (Q_b = 7.60 W). (c) Temperature distribution after 1 hour of discharging at 1C (Q_b = 7.60 W), using a flow rate at 0.20 L/min.

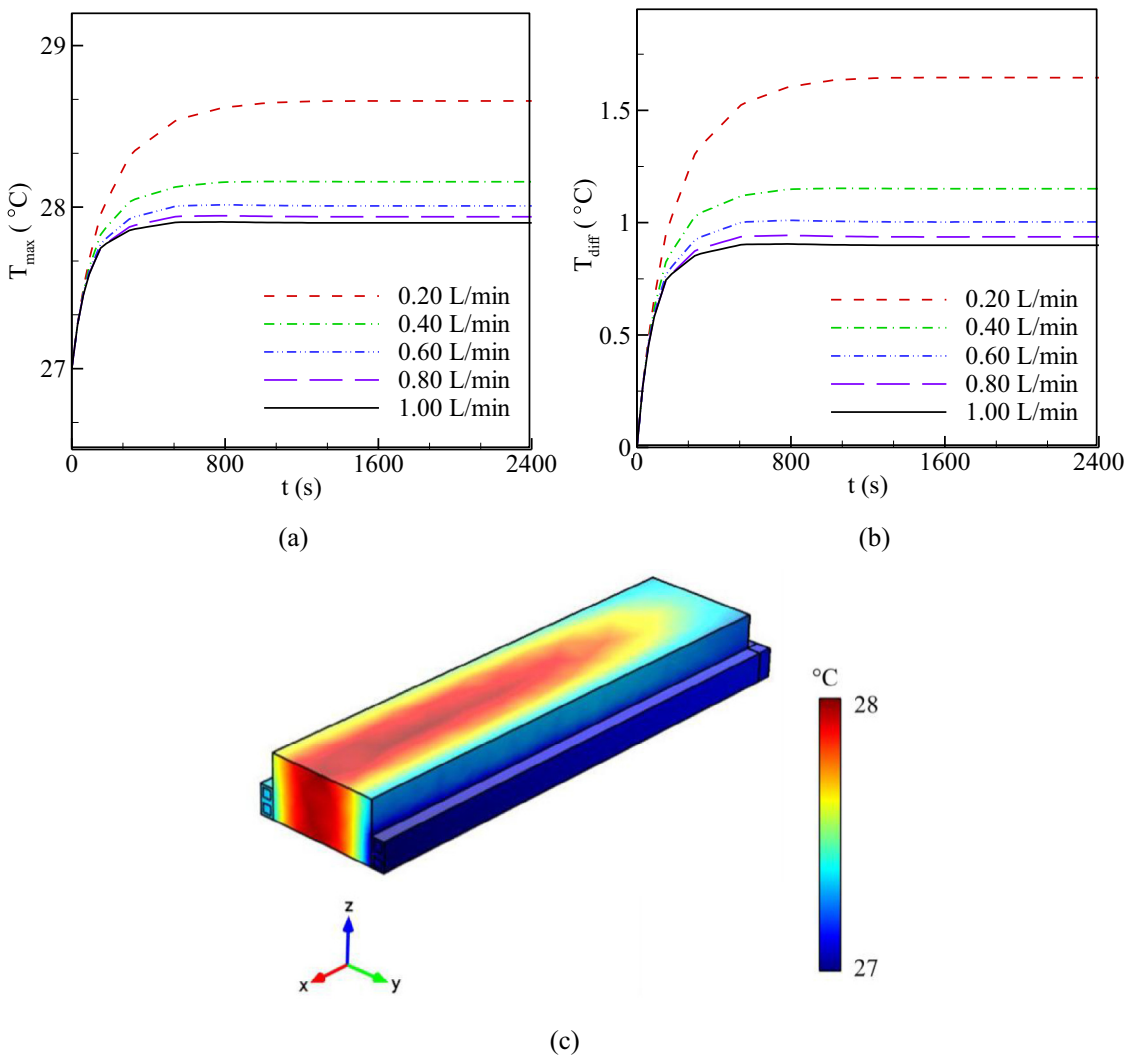

Fig. 6. Temporal history of (a) maximum temperature and (b) temperature difference using different flow rates, at a discharge rate of 1.5C (Q_b = 15.60 W). (c) Temperature distribution after 2400s of discharging at 1.5C (Q_b = 15.60 W), using a flow rate at 1.00 L/min.

at t = 2400 s. When the flow rate is further increased to 0.6 L/min, T_{max} reduces to 28.01 °C. Finally, when flow rate increases from 0.80 L/min to 1.00 L/min, T_{max} only reduces 0.04 °C and T_{uni} only reduces 3% while the required pumping power increases nearly twice as much as shown in Table 5. There is no more potential benefit by increasing the flow rate further, since the heat conduction rate inside the battery is limited by the material property, and the maximum temperature cannot be reduced any more by the minichannel cooling system. This will be explained in more detail in Subsection 3.3. Concerning the pumping power cost, 0.80 L/min is the best option for cooling performance at a discharge rate of 1.5C (Q_b = 15.60 W).

Table 5
Comparison of pressure drop, pumping power, temperature difference, maximum temperature and uniformity index using different flow rates at a discharge rate of 1.5C (Q_b = 15.60 W).

Flow rate (L/min)	ΔP (Pa)	Pumping power (W)	T_{diff} (°C)	T_{max} (°C)	T_{uni}
0.20	41.8	8.74e-6	1.65	28.66	0.058
0.40	160	6.66e-5	1.15	28.16	0.041
0.60	314	1.96e-4	1.00	28.01	0.036
0.80	508	4.23e-4	0.94	27.94	0.034
1.00	743	7.74e-4	0.90	27.90	0.033

3.3. *Thermal management at a discharge rate of 2C (Q_b = 23.89 W)*

A harsher situation is studied in this subsection as the discharge rate increases to 2C (Q_b = 23.89 W). According to the previous discussion for a discharge rate of 1.5C (Q_b = 15.60 W), flow rates at no less than 1.00 L/min are used for the cooling system performance analysis at a discharge rate of 2C.

Results for T_{max} and T_{diff} using different flow rates at a discharge rate of 2C (Q_b = 23.89 W) are shown in Fig. 7, respectively. At a flow rate of 1.00 L/min, T_{max} reaches to 28.38 °C. As flow rate increases to 2.00 L/min, T_{max} reduces to 28.27 °C, but the required pumping power becomes seven times larger (Table 6). When the flow rate increases further to 4.00 L/min, there is not much improvement for cooling performance as T_{max}, T_{diff} and T_{uni} remain almost unchanged. However, the pumping power is doubled to 3.61e-2 W. Concerning the pumping power cost, 2.00 L/min is the best option for cooling performance at a discharge rate of 2C (Q_b = 23.89 W).

To further explore the cooling system improvement using higher flow rate, the temperature contour of the battery and minichannels using a flow rate at 4.00 L/min is shown in Fig. 7(c). The temperature of the minichannels is quite low at both the inlet and the outlet, due to the large flow rate. The maximum battery temperature is at the center of the battery in the y (depth) direction, due to the low cross-plane thermal conductivity of the battery. Though the heat

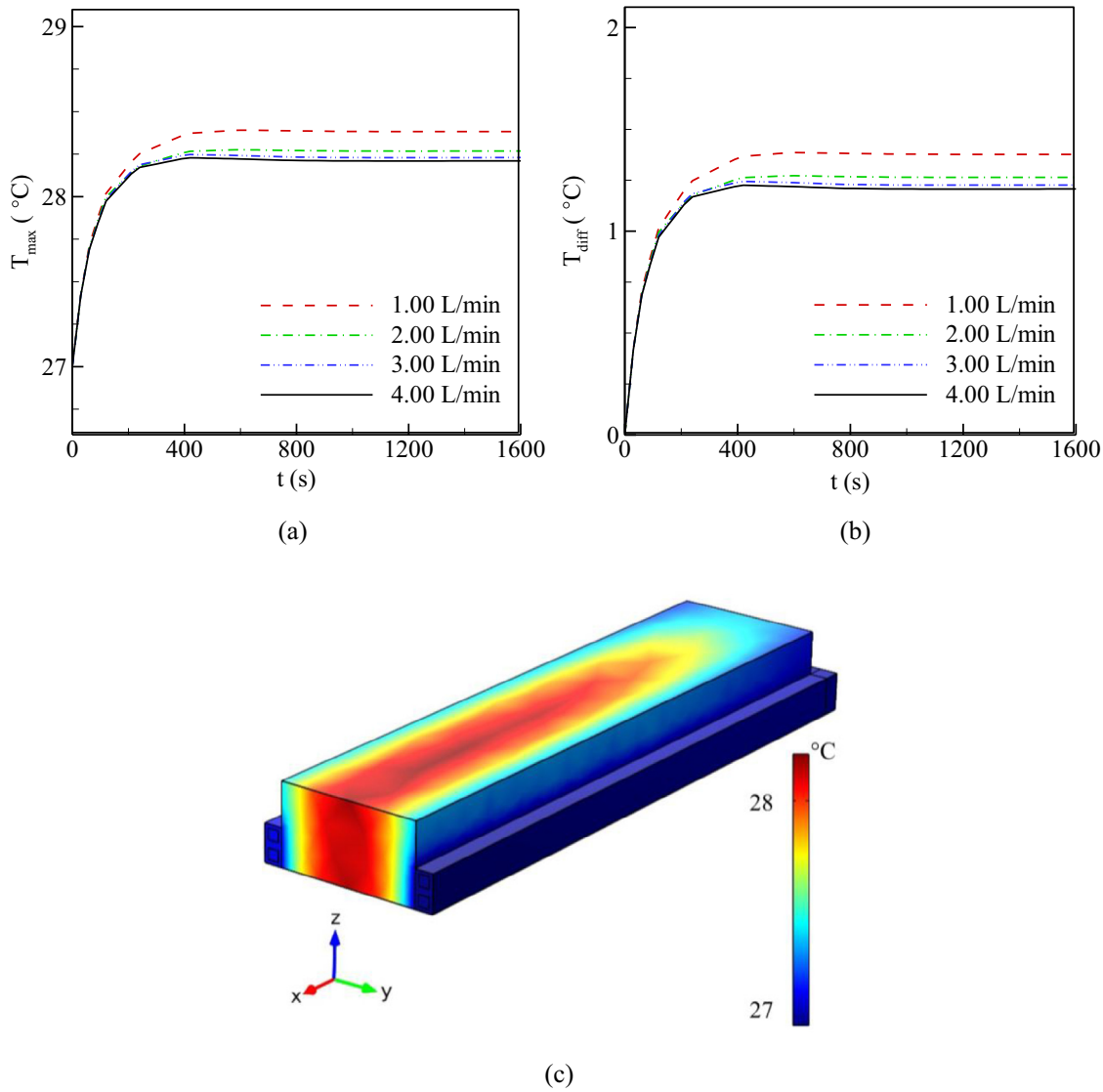

Fig. 7. Temporal history of (a) maximum temperature and (b) temperature difference using different higher flow rates, at a discharge rate of 2C (Q_b = 23.89 W). (c) Temperature distribution of battery and minichannels after 1800 s of discharging at 2C (Q_b = 23.89 W), using a flow rate at 4.00 L/min.

can be quickly taken away by the large flow rate, the heat transfer inside the battery is constraint by the (cross-plane) thermal conductivity of the material and the geometrical thickness in cross-plane (y) direction. Increasing the flow rates for the minichannels is not an effective solution for this high discharge rate. However, reducing the thickness of the cross-plane (y) direction should be an applicable solution. Though there is not much room to improve the cooling performance, maintaining T_{max} as low as 28.38 °C and T_{diff} as low as 1.38 °C is still acceptable for thermal management performance.

Table 6
Comparison of pressure drop, pumping power, temperature difference, maximum temperature and uniformity index using different flow rates at a discharge rate of 2C (Q_b = 23.89 W).

Flow rate (L/min)	ΔP (Pa)	Power (W)	T_{diff} (°C)	T_{max} (°C)	T_{uni}
1.00	743	7.74e-4	1.38	28.38	0.049
2.00	2.53k	5.27e-3	1.26	28.27	0.045
3.00	5.19k	1.63e-2	1.23	28.23	0.044
4.00	8.66k	3.61e-2	1.21	28.21	0.044

4. Conclusion

Parametric studies were carried out to demonstrate the feasibility of adopting the minichannels cooling system for high-capacity lithium-ion battery thermal management. Effects of different geometric designs, flow directions, and flow rates, were studied through parametric study by monitoring maximum temperature rise of the battery T_{max}, temperature difference across the battery T_{diff} and temperature uniformity T_{uni}. Under the same total flow rate inside the cooling system, the more minichannels are used, the better cooling performance can be achieved, though the inlet flow speed is reduced accordingly. Additionally, with the same total number of minichannels, the case using distributed distribution of minichannels shows better cooling performance than the case using concentrated distribution. Moreover, the effects of the flow rate and flow direction were studied. Results indicate that the best performance is achieved when all the flow inlets are aligned along one side of the battery, instead of alternating inlets and outlets.

In addition, this study shows that at a discharge rate of 1C, using a flow rate of 0.20 L/min, T_{max} is well controlled at 27.81 °C and T_{diff} is 0.80 °C after 1 hour of discharging, with only 8.69e-6 W pumping

power required. At a discharge rate of 1.5C, as flow rate increases to 0.80 L/min, T_{max} is 27.94 °C. Because only slight improvement on cooling performance can be achieved using flow rates higher than 0.80 L/min, 0.80 L/min is adopted as the best solution for cooling performance at a discharge rate of 1.5C, considering the pumping power cost for higher flow rates. When the discharge rate increases to 2C, at a flow rate of 1.00 L/min, T_{max} reaches to 28.27 °C and T_{diff} is 1.26 °C, with 5.27e-3 W pumping power required. Further increase in flow rate cannot reduce the temperature near the battery center in cross-plane (y) direction, but can only reduce the water temperature at the outlet.

In conclusion, we have demonstrated that the minichannels cooling system can be applied for the battery thermal management. This system can reduce both the maximum temperature rise and temperature difference across the whole battery, at little expense of pressure drop and pumping power.

Acknowledgement

This work was funded by the U.S. Department of Energy under the ARPA-E program (Award No. DEAR0000396).

References

[1] EPA, Global greenhouse gas emissions data. <http://www.epa.gov/climatechange/ghgemissions/global.html>, 2015 (accessed 07.09.15).
[2] J. Tollefson, Charging up the future, Nature 456 (2008) 436–440.
[3] S.F. Tie, C.W. Tan, A review of energy sources and energy management system in electric vehicles, Renew. Sustain. Energy Rev. 20 (2013) 82–102.
[4] T.M. Bandhauer, S. Garimella, T.F. Fuller, A critical review of thermal issues in lithium-ion batteries, J. Electrochem. Soc. 158 (2011) R1–R25.
[5] L.G. Lu, X. Han, J. Li, J. Hua, M. Ouyang, A review on the key issues for lithium-ion battery management in electric vehicles, J. Power Sources 226 (2013) 272–288.
[6] Z.H. Rao, S.F. Wang, A review of power battery thermal energy management, Renew. Sustain. Energy Rev. 15 (2011) 4554–4571.
[7] Q. Wang, P. Ping, X. Zhao, G. Chu, J. Sun, C. Chen, Thermal runaway caused fire and explosion of lithium ion battery, J. Power Sources 208 (2012) 210–224.
[8] R. Spotnitz, J. Franklin, Abuse behavior of high-power, lithium-ion cells, J. Power Sources 113 (2003) 81–100.
[9] P. Balakrishnan, R. Ramesh, T.P. Kumar, Safety mechanisms in lithium-ion batteries, J. Power Sources 155 (2006) 401–414.
[10] L. Lu, X. Han, J. Li, J. Hua, M. Ouyang, A review on the key issues for lithium-ion battery management in electric vehicles, J. Power Sources 226 (2013) 272–288.
[11] A.A. Pesaran, Battery thermal models for hybrid vehicle simulations, J. Power Sources 110 (2002) 377–382.
[12] S. Chen, C.C. Wan, Y.Y. Wang, Thermal analysis of lithium-ion batteries, J. Power Sources 140 (2005) 111–124.
[13] T. Hatchard, D.D. MacNeil, A. Basu, J.R. Dahn, Thermal model of cylindrical and prismatic lithium-ion cells, J. Electrochem. Soc. 148 (2001) A755–A761.
[14] G.H. Kim, A. Pesaran, R. Spotnitz, A three-dimensional thermal abuse model for lithium-ion cells, J. Power Sources 170 (2007) 476–489.
[15] G. Guo, B. Long, B. Cheng, S. Zhou, P. Xu, B. Cao, Three-dimensional thermal finite element modeling of lithium-ion battery in thermal abuse application, J. Power Sources 195 (2010) 2393–2398.
[16] K. Smith, C.Y. Wang, Power and thermal characterization of a lithium-ion battery pack for hybrid-electric vehicles, J. Power Sources 160 (2006) 662–673.
[17] H. Sun, X. Wang, B. Tossan, R. Dixon, Three-dimensional thermal modeling of a lithium-ion battery pack, J. Power Sources 206 (2012) 349–356.
[18] C.H. Doh, D.H. Kim, H.S. Kim, H.M. Shin, Y.D. Jeong, S.I. Moon, et al., Thermal and electrochemical behaviour of C/Li x CoO 2 cell during safety test, J. Power Sources 175 (2008) 881–885.
[19] K.C. Chiu, C.H. Lin, S.F. Yeh, Y.H. Lin, K.C. Chen, An electrochemical modeling of lithium-ion battery nail penetration, J. Power Sources 251 (2014) 254–263.
[20] U.S. Kim, J. Yi, C.B. Shin, T. Han, S. Park, Modelling the thermal behaviour of a lithium-ion battery during charge, J. Power Sources 196 (2011) 5115–5121.
[21] M.S. Wu, K.H. Liu, Y.Y. Wang, C.C. Wan, Heat dissipation design for lithium-ion batteries, J. Power Sources 109 (2002) 160–166.
[22] X. Xu, R. He, Review on the heat dissipation performance of battery pack with different structures and operation conditions, Renew. Sustain. Energy Rev. 29 (2014) 301–315.
[23] R. Mahamud, C. Park, Reciprocating air flow for Li-ion battery thermal management to improve temperature uniformity, J. Power Sources 196 (2011) 5685–5696.
[24] T. Wang, K.J. Tseng, J. Zhao, Z. Wei, Thermal investigation of lithium-ion battery module with different cell arrangement structures and forced air-cooling strategies, Appl. Energy 134 (2014) 229–238.
[25] S.K. Mohammadian, Y. Zhang, Thermal management optimization of an air-cooled Li-ion battery module using pin-fin heat sinks for hybrid electric vehicles, J. Power Sources 273 (2015) 431–439.
[26] L. Fan, J.M. Khodadadi, A.A. Pesaran, A parametric study on thermal management of an air-cooled lithium-ion battery module for plug-in hybrid electric vehicles, J. Power Sources 238 (2013) 301–312.
[27] R. Sabbah, R. Kizilel, J.R. Selman, S. Al-Hallaj, Active (air-cooled) vs. passive (phase change material) thermal management of high power lithium-ion packs: limitation of temperature rise and uniformity of temperature distribution, J. Power Sources 182 (2008) 630–638.
[28] S. Al Hallaj, J. Selman, A novel thermal management system for electric vehicle batteries using phase-change material, J. Electrochem. Soc. 147 (2000) 3231–3236.
[29] S. Al-Hallaj, J. Selman, Thermal modeling of secondary lithium batteries for electric vehicle/hybrid electric vehicle applications, J. Power Sources 110 (2002) 341–348.
[30] R. Kizilel, R. Sabbah, J.R. Selman, S. Al-Hallaj, An alternative cooling system to enhance the safety of Li-ion battery packs, J. Power Sources 194 (2009) 1105–1112.
[31] Z. Rao, S. Wang, A review of power battery thermal energy management, Renew. Sustain. Energy Rev. 15 (2011) 4554–4571.
[32] Y. Zhang, X.L. Yu, Q.K. Feng, R.T. Zhang, Thermal performance study of integrated cold plate with power module, Appl. Therm. Eng. 29 (2009) 3568–3573.
[33] L. Jin, P.S. Lee, X.X. Kong, Y. Fan, S.K. Chou, Ultra-thin minichannel LCP for EV battery thermal management, Appl. Energy 113 (2014) 1786–1794.
[34] Y. Huo, Z. Rao, X. Liu, J. Zhao, Investigation of power battery thermal management by using mini-channel cold plate, Energy Convers. Manag. 89 (2015) 387–395.
[35] X. Xie, Z.J. Liu, Y.L. He, W.Q. Tao, Numerical study of laminar heat transfer and pressure drop characteristics in a water-cooled minichannel heat sink, Appl. Therm. Eng. 29 (2009) 64–74.
[36] J.P. Rugh, A. Pesaran, K. Smith, Electric vehicle battery thermal issues and thermal management techniques, presented at the SAE 2011 Alternative Refrigerant and System Efficiency Syposium, 2011.
[37] R.K. Shah, A.L. London, Laminar Flow Forced Convection in Ducts: A Source Book for Compact Heat Exchanger Analytical Data, vol. 1, Cambridge, MA, Academic Press, 1978.
[38] D. Liu, S.V. Garimella, Investigation of liquid flow in microchannels, J. Thermophys. Heat Transfer 18 (2004) 65–72.
[39] M.V. Koch, K.M. VandenBussche, R.W. Chrisman, Micro Instrumentation: For High Throughput Experimentation and Process Intensification – A Tool for PAT, Hoboken, NJ, John Wiley & Sons, 2007.